Coupling Lattice Instabilities across the Interface in Ultrathin Oxide Heterostructures

Van Thiel, Thierry C.; Fowlie, Jennifer; Autieri, Carmine; Manca, Nicola; Šiškins, Makars; Afanasiev, Dmytro; Gariglio, Stefano; Caviglia, Andrea D.

Important note
To cite this publication, please use the final published version (if applicable).
Please check the document version above.

Coupling Lattice Instabilities Across the Interface in Ultrathin Oxide Heterostructures

Thierry C. van Thiel,* Jennifer Fowlie, Carmine Autieri, Nicola Manca, Makars Šiškins, Dmytro Afanasiev, Stefano Gariglio, and Andrea D. Caviglia

Read Online

ACCESS | Metrics & More | Article Recommendations | SI Supporting Information

ABSTRACT: Oxide heterointerfaces constitute a rich platform for realizing novel functionalities in condensed matter. A key aspect is the strong link between structural and electronic properties, which can be modified by interfacing materials with distinct lattice symmetries. Here, we determine the effect of the cubic-tetragonal distortion of $SrTiO_3$ on the electronic properties of thin films of $SrIrO_3$, a topological crystalline metal hosting a delicate interplay between spin-orbit coupling and electronic correlations. We demonstrate that below the transition temperature at 105 K, $SrIrO_3$ orthorhombic domains couple directly to tetragonal domains in $SrTiO_3$. This forces the in-phase rotational axis to lie in-plane and creates a binary domain structure in the $SrIrO_3$ film. The close proximity to the metal−insulator transition in ultrathin $SrIrO_3$ causes the individual domains to have strongly anisotropic transport properties, driven by a reduction of bandwidth along the in-phase axis. The strong structure−property relationships in perovskites make these compounds particularly suitable for static and dynamic coupling at interfaces, providing a promising route towards realizing novel functionalities in oxide heterostructures.
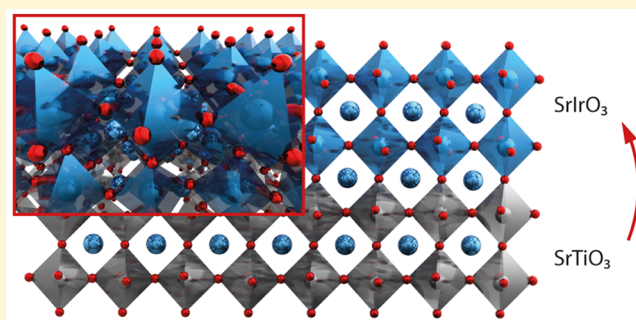
Engineering matter with tailored properties is one of the main objectives in materials science. Perovskite oxides have been at the center of attention due to the combination of a flexible lattice structure and strong structure-property relationships. At heterointerfaces, structural phases and domain patterns that are not present in bulk can manifest.[1−3] Such artificial phases can have a marked effect on electronic and magnetic properties and have been shown to modify features, such as magnetic anisotropy,[4,5] interfacial ferromagnetism,[6−8] and ferroelectricity.[9] Recent years have seen an increasing amount of attention focused on the exploration of nanoscale domains, which have emerged as an abundant source of novel physical properties.[10−14] Control of such domain patterns, however, remains an open challenge. A possible way forward is to incorporate materials that undergo structural phase transitions. A canonical example is $SrTiO_3$, a widely used material that undergoes a transition from a cubic to a tetragonal phase when lowering the temperature below 105 K. At this temperature, $SrTiO_3$ breaks up into ferroelastic domains in which TiO_6 octahedra rotate about one of three possible directions.[15] When $SrTiO_3$ is used as a substrate for heteroepitaxial growth, the rotational distortion and resulting domain pattern can interact with the thin film due to octahedral connectivity across the interface.[16] In this context, semimetal $SrIrO_3$ is of particular interest, since dimensionality

and octahedral rotations have been shown to be pivotal in the delicate interplay between spin-orbit coupling (SOC) and electronic correlations.[17−19] Efforts to study $SrIrO_3$ have primarily been fueled by theoretical predictions of a Dirac nodal ring, which is at the boundary between multiple topological classes, depending on the type of lattice symmetry-breaking.[20−22] In this respect, the interplay between the correlation strength and electronic bandwidth is crucial as it determines the position of the Dirac point with respect to the Fermi level.[17,21,23] The bandwidth is, among other things, governed by the Ir−O−Ir bond angle, which may be controlled through cation substitution, pressure tuning,[24] or hetero-epitaxy.

Here, we demonstrate manipulation of the structural domain pattern of $SrIrO_3$ thin films, through interaction with the tetragonal distortion in $SrTiO_3$. We find that tetragonal domains in the substrate couple directly to orthorhombic domains in the film, forcing a binary domain structure in

SrIrO$_3$. In ultrathin films, the SrTiO$_3$ tetragonal distortion induces a strong anisotropy in the longitudinal resistivity of SrIrO$_3$, manifesting as a metal-to-insulator transition. Ab initio calculations on ultrathin films corroborate the anisotropic character of the domains, revealing a depletion of states at the Fermi level along one lattice axis, while along the other the system remains metallic.

The resistivity (ρ) versus temperature (T) characteristics of three SrIrO$_3$/SrTiO$_3$ heterostructures measured in a Hall bar (HB) geometry are shown in Fig. 1a. The film thicknesses were
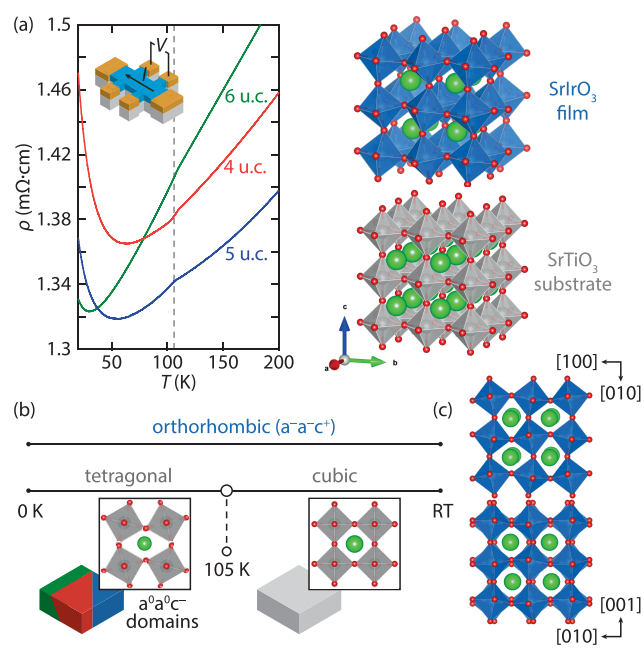

Figure 1. Simultaneous structural and electronic transition. (a) ρ (T) curves of SrIrO$_3$ films of different thicknesses, measured in a HB geometry oriented along the (100) lattice axis. (b) Bulk phase diagram of SrIrO$_3$ and SrTiO$_3$. Perovskite SrIrO$_3$ is orthorhombic at all temperatures, while SrTiO$_3$ undergoes a transition from a cubic to a tetragonal phase below 105 K. (c) Octahedral rotations and cation displacements of orthorhombic SrIrO$_3$ viewed along the pseudocubic [001] (top) and [100] (bottom) directions.

chosen to be just above the critical point for the metal–insulator transition,[18] such that the properties of the films are most sensitive to interface effects while maintaining a semimetallic ground state. At $T = 105$ K, ρ displays a sudden change of slope. Note that the change in resistivity of the SrIrO$_3$ film occurs simultaneously with the structural phase-transition in the SrTiO$_3$ substrate, indicating a strong octahedral connectivity across the interface that couples the lattice degrees of freedom of the SrTiO$_3$ substrate to the electronic properties of the SrIrO$_3$ film. The bulk phase diagrams and lattice structures of SrIrO$_3$ and SrTiO$_3$ are shown in Figure 1b and 1c.[25] Perovskite SrIrO$_3$ has an orthorhombic structure (space group $Pbnm$) from 300 K down to low temperature, with rotation angles of typically 10° or larger about the pseudocubic lattice axes.[26,27] SrTiO$_3$ is cubic ($Pm\bar{3}m$) but transforms into a tetragonal phase ($I4mcm$) below 105 K, where it forms three possible domains. Its transition temperature, as well as the magnitude of the distortion can be controlled by, for example, Ca- or Ba-doping.[28−30]

Octahedral rotations double the perovskite unit cell, a phenomenon that gives rise to half-order Bragg peaks in X-ray diffraction measurements. The presence of specific half-order peaks is governed by symmetry,[31] and the measurement of a set of half-order peaks can be used to fully determine the rotational pattern of the film.[32] SrTiO$_3$ is characterized by $a^0a^0c^-$, that is, an out-of-phase rotation about the c-axis, which is slightly elongated.[33] Bulk SrIrO$_3$ is denoted by $a^-a^-c^+$, having out-of-phase rotations of the same amplitude about two axes and in-phase rotations of different amplitude about the third axis.[34] To study the octahedral rotations in the SrIrO$_3$/SrTiO$_3$ heterostructures, we performed low temperature (4 K) synchrotron X-ray diffraction measurements. The films have thicknesses of 40, 25, and 15 u.c. and are capped by an amorphous SrTiO$_3$ layer, preventing an additional diffraction signal from the capping layer while shielding the film from exposure to ambient conditions. Measurements of the (002) diffraction peak of these films are shown in Figure 2a, which
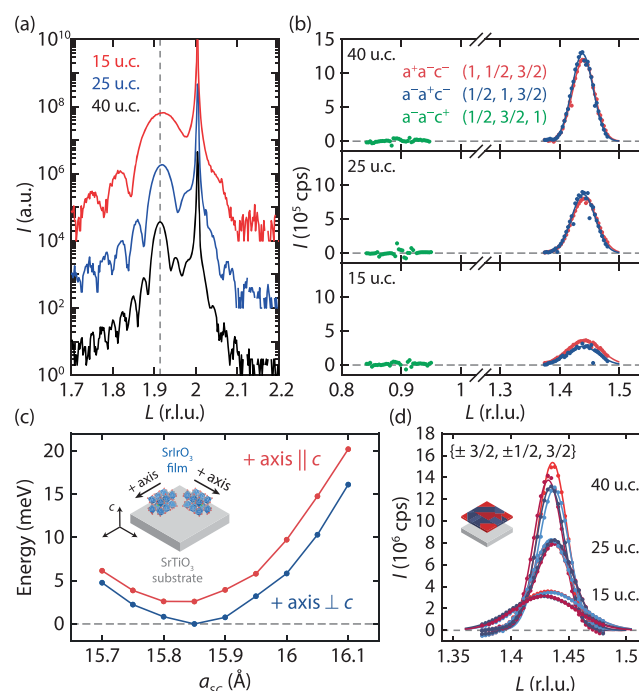

Figure 2. Binary domain structure. (a) XRD L-scans of SrIrO$_3$ films of different thicknesses, measured in the vicinity of the (002) reflection of the SrTiO$_3$ substrate. (b) Half-order peaks arising from in-phase octahedral rotations. (c) DFT calculated energy difference per formula unit for the in-phase axis (red) parallel and (blue) perpendicular to the c-axis (growth axis) as a function of lattice constant for supercells consisting of four formula units of SrTiO$_3$ and SrIrO$_3$. (d) Half-order peaks from different rotational domains.

demonstrate that the films are compressively strained. We first consider (h, k, l) Bragg conditions where one of the three reciprocal lattice positions is an integer and the other two are unequal half-order positions (1/2, 1, 3/2). This peak is present if the integer reciprocal lattice vector is parallel to the real-space direction of the in-phase axis.[35] As shown in Figure 2b, a peak is present when the integer reciprocal lattice vector is along h and k, but not along l. From this, we infer that the in-phase rotation (+) axis lies in the plane of the film, and it exhibits a mixed population of $a^+a^-c^-$ and $a^-a^+c^-$ domains,
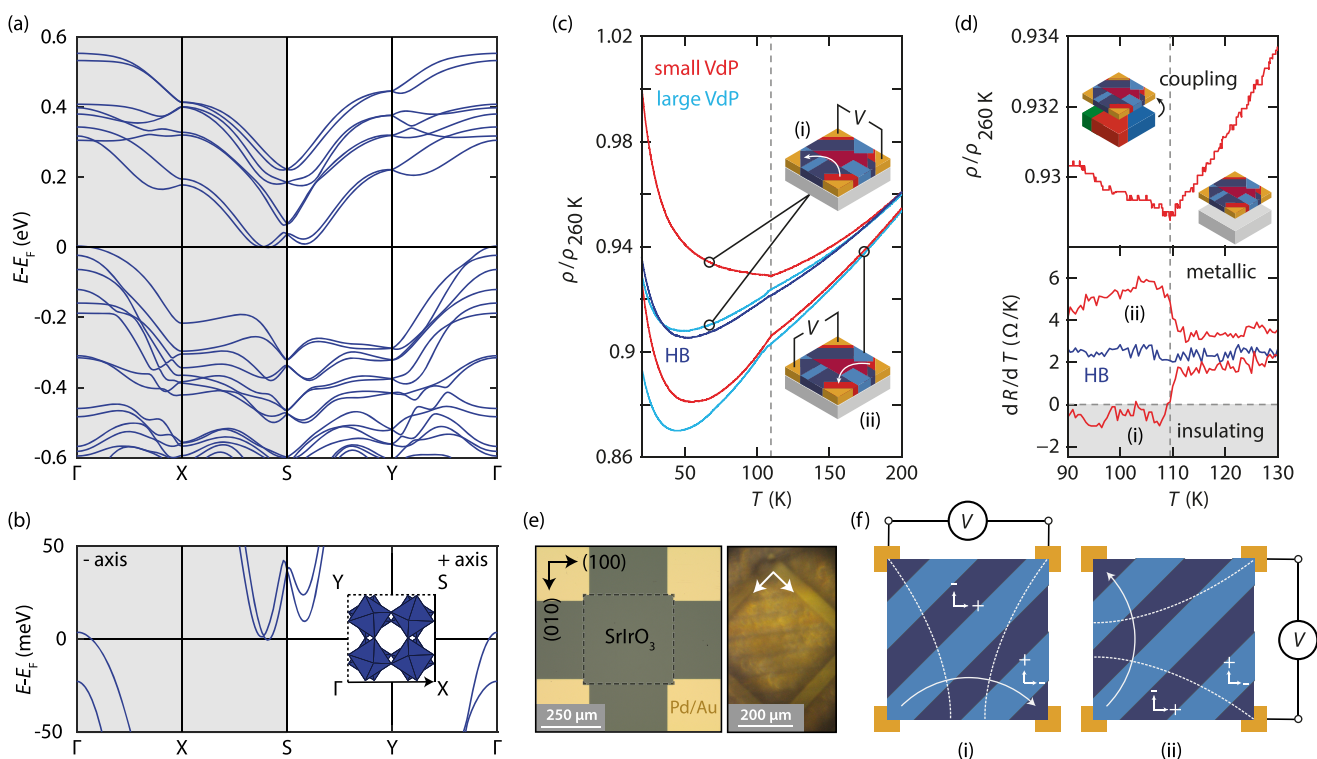
Figure 3. Anisotropic electronic transport. (a) DFT-calculated band structure with the out-of-phase (−) axis along Γ−X and the in-phase (+) axis along Γ−Y. (b) Enlarged view around the Fermi energy. The inset shows the Brillouin zone of the primitive orthorhombic unit cell. (c) ρ (T) curves of a 5 u.c. film comparing (light blue) a large (750 μm) and (red) small (375 μm) VdP geometry, measured in two mutually orthogonal configurations of current and voltage probes. The dark blue curve represents the ρ (T) curve recorded in a 150 μm wide Hall bar (aspect ratio 3:1). (d) Enlarged view of ρ (T) around the cubic-to-tetragonal transition of $SrTiO_3$ at 105 K (top) and the corresponding dρ/dT curves (bottom). (e) Optical microscope images of (left) the 375 μm VdP device and (right) $c^- a^0 a^0$ and $a^0 c^- a^0$ tetragonal domains in $SrTiO_3$ in a 375 μm square area. (f) Illustration of current traversing a binary domain population in the probing region of the device.

consistent with previous reports.[17,36] In the ABO_3 *Pbnm* structure, the B−B distance, along the in-phase axis is slightly shorter compared to the out-of-phase axis. Therefore, to minimize the lattice mismatch with the compressive substrate, the in-phase axis should lie in-plane. The a^- axis, which experiences the largest strain, should then be oriented along the c^- axis of $SrTiO_3$ tetragonal domains, such that $a^- a^+ c^-$ ($a^+ a^- c^-$) domains in the film couple to $c^- a^0 a^0$ ($a^0 c^- a^0$) domains in the substrate. This is supported by *ab initio* calculations (Figure 2c), which show (1) that forming $a^- a^- c^+$ domains is energetically unfavorable due to a larger in-plane lattice parameter when the in-phase axis is oriented out-of-plane (a_{pc} = 3.9430 Å) as compared to in-plane (a_{pc} = 3.9411 Å)[26] and (2) that the energy is minimized for the aforementioned domain configuration (see section VI of the Supporting Information for further details). Different rotational domains arise depending on whether the octahedron closest to the origin rotates clockwise or counterclockwise about each axis. This is probed by the {1/2, 1/2, 3/2} series of half-order peaks, which provide the a (or b) direction along which the displacement of Sr ions occurs. Peaks are present for all reflection conditions (Figure 2d), indicating that the $SrIrO_3$ film consists of two orthorhombic domains with a aligned along [100] and [010].

Having established a coupling between the binary domain structure in the $SrIrO_3$ film and the tetragonal domains in the $SrTiO_3$ substrate, we turn to the question of how this interfacial domain coupling affects the electronic properties and the connection with the observed anomaly in the ρ−T

curve. While in the *Pbnm* structure, the B−B distance along the in-phase axis is shorter compared to the out-of-phase axis, the B−O−B bond angles are slightly more tilted.[37] Accordingly, one would expect a reduction of bandwidth along the in-phase axis due to a reduced orbital overlap,[38] with anisotropic transport properties as a consequence. Figure 3a and 3b show the DFT-calculated electronic structure, assuming a correlation strength U = 1.47 eV, similar to previous work.[18] The out-of-phase (−) axis is oriented along Γ−X and the in-phase (+) axis along Γ−Y, with Γ the center of the primitive orthorhombic Brillouin zone. Electron wavepackets along Γ−X have a group velocity oriented purely along the out-of-phase axis and along X−S include a component along the in-phase axis, which is smaller than or equal to the component along the out-of-phase axis. Accordingly, Γ−X−S (gray region) comprises carrier transport oriented either fully or predominantly along the out-of-phase axis (and analogously for S−Γ−Y and the in-phase axis). Two electron-like pockets are present along X−S and S−Y. However, only the former intersects the Fermi level and the latter remains unoccupied. As a consequence, electronic bands along the in-phase axis are depleted at the Fermi level and the system is anticipated to favor insulating behavior along the in-phase axis but remain metallic along the out-of-phase axis. This is a remarkable scenario, where the electronic structure is finely tuned between a metallic and insulating phase by a reduction of bandwidth along the in-phase axis. In $AIrO_3$ iridates, time-reversal symmetry protects the nodal line and thus safeguards metallic behavior. A metal−insulator transition, therefore, necessarily coincides with the onset of *G*-type antiferromag-

netic order.[18,22,39] Our DFT calculations confirm that AFM is required to realize any type of insulating behavior, even if it is anisotropic in nature. Experimentally, we indeed observe strongly anisotropic electronic properties. Figure 3c shows ρ (T) measured in a HB geometry and in two patterned van der Pauw (VdP) squares with sizes of 375 and 750 μm for two electrical configurations. We directly observe that the anomaly in ρ is much more pronounced in the VdP geometry than in the Hall bar and that a strong anisotropy develops below 105 K. As shown in Figure 3d, the transition can be remarkably sharp and manifest as a metal-insulator transition. The derivative $\mathrm{d}\rho/\mathrm{d}T$ is shown in the bottom panel, which shows opposite behavior in the two electrical configurations, that is, a positive (metallic) or negative (insulating) slope depending on the orientation. Microscopically, this can be viewed as current traversing an unequal domain population in the probing region of the VdP device (see Figure 3e and 3f). Domains in SrTiO$_3$ can be sized up to 100 μm (see also section IV of the Supporting Information), which suggests, in accordance with our observations, that the anisotropic character should be most pronounced in small devices and reduced in larger devices due to statistical averaging over complex domain patterns.[11,12,40] The ρ (T) anomaly at 105 K can then be ascribed to a sudden reconfiguration of the current paths as the SrIrO$_3$ domains adapt to the onset of the tetragonal multi-domain state of the SrTiO$_3$ substrate. We remark that at the boundaries between adjacent structural domains, the crystal unit cells are typically distorted.[12] Considering the strong structure-property relationship in iridates, it is likely that the domain walls have different electronic properties compared to the undistorted areas. However, because of the ~45° angle with respect to the crystal lattice axes, any enhanced or suppressed conductivity would be projected equally onto the (100) and (010) directions. Hence, the devices shown in Figure 3 are only sensitive to the domains and not to the domain walls. Probing transport in nanoscale devices oriented at 45° could elucidate their electronic properties.

To further explore the effect of the SrTiO$_3$ tetragonal distortion on the octahedral rotations in SrIrO$_3$, we performed temperature-dependent diffraction measurements across the transition temperature (see Figure 4). By fitting the half-order Bragg peaks with a Gaussian function and comparing the areas under the curves, we quantify the octahedral rotation angles and cation displacements as a function of temperature.[41] The oxygen positions are obtained by comparing the intensities of the peaks with the calculated structure factor of the oxygen octahedra. Standard nonlinear regression is used to determine the optimal values of α and γ, defined in Figure 4. The determined in- and out-of-plane rotation angles α and γ, respectively, are plotted versus temperature for SrIrO$_3$ films of different thicknesses in Figure 4a. The angles are found to be nearly constant over the entire temperature range and weakly dependent on the film thickness (Figure 4b). Figure 4c visualizes the low temperature lattice structure. The rotational angles are substantially reduced with respect to bulk SrIrO$_3$. Considering that SrTiO$_3$ has been reported to strongly suppress octahedral rotations in other oxide heterostructures,[4] we attribute this to the interaction with the SrTiO$_3$ substrate.[42] We also find an enhancement of orthorhombicity for the thinner films, possibly pointing to larger rotational distortions in the unit cells closest to the SrTiO$_3$/SrIrO$_3$ interface (see also section VI of the Supporting Information). Interestingly, we do not observe a clear deviation of the SrIrO$_3$ rotation
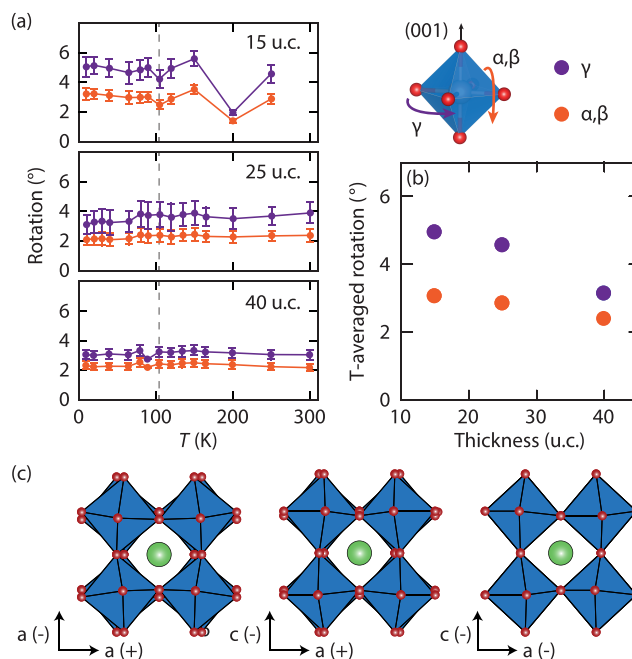

Figure 4. Temperature dependence of octahedral rotations. (a) Rotation angles of the 15, 25, and 40 u.c. films as a function of temperature. (b) Temperature-averaged rotation angles as a function of film thickness. (c) Visualization of the octahedral rotation pattern as seen (from left to right) along the c^-, a^-, and a^+ axes, respectively.

angles across 105 K, further pointing to the reconfiguration of the multi-domain state as the underlying cause of the observed resistivity anomaly at 105 K.

In summary, we established an interfacial coupling in ultrathin SrTiO$_3$/SrIrO$_3$ heterostructures and demonstrated the emergence of a binary orthorhombic domain pattern in SrIrO$_3$ that couples directly to the tetragonal domains in the SrTiO$_3$ substrate. For each domain, the electronic bandwidth along the in-phase rotational axis is suppressed, resulting in strongly anisotropic transport properties that manifest as a metal-insulator transition. This coupling mechanism is not limited to iridates, but can be extended to control physical properties, such as magnetism, multiferroicity, and superconductivity in a wide variety of orthorhombic materials, for example, ferrites, manganites, and nickelates.[43−49]

■ EXPERIMENTAL METHODS

SrIrO$_3$ thin films were synthesized by pulsed-laser deposition on (001) TiO$_2$-terminated SrTiO$_3$ substrates. The growth conditions are described in detail in previous work, including the requirement of a protective capping layer to prevent degradation of the films resulting from exposure to ambient conditions.[50] Samples measured in transport were capped by a 10 u.c. crystalline layer of SrTiO$_3$, whereas samples measured in XRD were capped by amorphous SrTiO$_3$, to prevent an additional contribution in diffraction. Hall bar (HB) and van der Pauw (VdP) geometries were patterned by e-beam lithography. The SrIrO$_3$ layer was contacted by Ar etching and in situ deposition of Pd and Au, resulting in low-resistance Ohmic contacts (see also section V.A of the Supporting Information). Low temperature transport measurements were performed in an Oxford flow cryostat, by sourcing a low frequency (~17 Hz) 10 μA current and measuring the

resulting voltage with a lock-in amplifier. Details regarding the synchrotron X-ray diffraction measurements, half-order peak analysis, polarized-light microscopy measurements and ab initio calculations are described in the Supporting Information.

■ ASSOCIATED CONTENT

Ⓢⓘ Supporting Information

The Supporting Information is available free of charge at https://pubs.acs.org/doi/10.1021/acsmaterialslett.9b00540.

Crystallographic data from the DFT structural relaxation (CIF)

Description of the determination of the octahedral rotation angles, X-ray diffraction data of rotational distortions in$SrTiO_3$ above the condensation point, additional diffraction measurements on ultrathin $SrIrO_3$ films, imaging of tetragonal domains in $SrTiO_3$, description of the device fabrication and additional transport measurements on a 30 u.c. film, and additional ab initio calculations (PDF)

■ AUTHOR INFORMATION

Corresponding Author

Thierry C. van Thiel − *Kavli Institute of Nanoscience, Delft University of Technology, 2628 CJ Delft, Netherlands;* ⓞ orcid.org/0000-0003-4396-5227; Email: t.c.vanthiel@tudelft.nl

Authors

Jennifer Fowlie − *Department of Quantum Matter Physics, University of Geneva, 1211 Genève 4, Switzerland;* ⓞ orcid.org/0000-0002-3528-6390

Carmine Autieri − *International Research Centre MagTop, Institute of Physics, Polish Academy of Sciences, PL-02668 Warsaw, Poland; Consiglio Nazionale delle Ricerche, Istituto Superconduttori, Materiali Innovativi e Dispositivi (CNR-SPIN), I-66100 Chieti, Italy*

Nicola Manca − *Kavli Institute of Nanoscience, Delft University of Technology, 2628 CJ Delft, Netherlands*

Makars Šiškins − *Kavli Institute of Nanoscience, Delft University of Technology, 2628 CJ Delft, Netherlands;* ⓞ orcid.org/0000-0003-4295-2221

Dmytro Afanasiev − *Kavli Institute of Nanoscience, Delft University of Technology, 2628 CJ Delft, Netherlands*

Stefano Gariglio − *Department of Quantum Matter Physics, University of Geneva, 1211 Genève 4, Switzerland*

Andrea D. Caviglia − *Kavli Institute of Nanoscience, Delft University of Technology, 2628 CJ Delft, Netherlands*

Complete contact information is available at:
https://pubs.acs.org/10.1021/acsmaterialslett.9b00540

Notes

The authors declare no competing financial interest.

■ ACKNOWLEDGMENTS

■ REFERENCES

(1) Rondinelli, J. M.; May, S. J.; Freeland, J. W. Control of octahedral connectivity in perovskite oxide heterostructures: An emerging route to multifunctional materials discovery. *MRS Bull.* **2012**, 37, 261−270.

(2) Kan, D.; Aso, R.; Kurata, H.; Shimakawa, Y. Research Update: Interface-engineered oxygen octahedral tilts in perovskite oxide heterostructures. *APL Mater.* **2015**, 3, 062302.

(3) Liao, Z.; Green, R. J.; Gauquelin, N.; Macke, S.; Li, L.; Gonnissen, J.; Sutarto, R.; Houwman, E. P.; Zhong, Z.; Van Aert, S. e. a. Long-Range Domain structure and symmetry engineering by interfacial oxygen octahedral coupling at heterostructure interface. *Adv. Funct. Mater.* **2016**, 26, 6627−6634.

(4) Liao, Z.; Huijben, M.; Zhong, Z.; Gauquelin, N.; Macke, S.; Green, R.; Van Aert, S.; Verbeeck, J.; Van Tendeloo, G.; Held, K.; et al. Controlled lateral anisotropy in correlated manganite heterostructures by interface-engineered oxygen octahedral coupling. *Nat. Mater.* **2016**, 15, 425−431.

(5) Kan, D.; Aso, R.; Sato, R.; Haruta, M.; Kurata, H.; Shimakawa, Y. Tuning magnetic anisotropy by interfacially engineering the oxygen coordination environment in a transition metal oxide. *Nat. Mater.* **2016**, 15, 432−437.

(6) Grutter, A. J.; Vailionis, A.; Borchers, J. A.; Kirby, B. J.; Flint, C.; He, C.; Arenholz, E.; Suzuki, Y. Interfacial symmetry control of emergent ferromagnetism at the nanoscale. *Nano Lett.* **2016**, 16, 5647−5651.

(7) Guo, H.; Wang, Z.; Dong, S.; Ghosh, S.; Saghayezhian, M.; Chen, L.; Weng, Y.; Herklotz, A.; Ward, T. Z.; Jin, R.; et al. Interface-induced multiferroism by design in complex oxide superlattices. *Proc. Natl. Acad. Sci. U. S. A.* **2017**, 201706814.

(8) Paul, A.; Reitinger, C.; Autieri, C.; Sanyal, B.; Kreuzpaintner, W.; Jutimoosik, J.; Yimnirun, R.; Bern, F.; Esquinazi, P.; Korelis, P.; et al. Exotic exchange bias at epitaxial ferroelectric-ferromagnetic interfaces. *Appl. Phys. Lett.* **2014**, 105, 022409.

(9) Kim, Y.-M.; Kumar, A.; Hatt, A.; Morozovska, A. N.; Tselev, A.; Biegalski, M. D.; Ivanov, I; Eliseev, E. A.; Pennycook, S. J.; Rondinelli, J. M.; et al. Interplay of octahedral tilts and polar order in BiFeO3 films. *Adv. Mater.* **2013**, 25, 2497−2504.

(10) Seidel, J.; Martin, L. W.; He, Q.; Zhan, Q.; Chu, Y.-H.; Rother, A.; Hawkridge, M.; Maksymovych, P.; Yu, P.; Gajek, M. e. a.; et al. Conduction at domain walls in oxide multiferroics. *Nat. Mater.* **2009**, 8, 229.

(11) Kalisky, B.; Spanton, E. M.; Noad, H.; Kirtley, J. R.; Nowack, K. C.; Bell, C.; Sato, H. K.; Hosoda, M.; Xie, Y.; Hikita, Y.; et al. Locally enhanced conductivity due to the tetragonal domain structure in LaAlO3/SrTiO3 heterointerfaces. *Nat. Mater.* **2013**, 12, 1091.

(12) Honig, M.; Sulpizio, J. A.; Drori, J.; Joshua, A.; Zeldov, E.; Ilani, S. Local electrostatic imaging of striped domain order in LaAlO3/SrTiO3. *Nat. Mater.* 2013, 12, 1112.

(13) Chauleau, J.-Y.; Chirac, T.; Fusil, S.; Garcia, V.; Akhtar, W.; Tranchida, J.; Thibaudeau, P.; Gross, I.; Blouzon, C.; Finco, A. e. a. Electric and antiferromagnetic chiral textures at multiferroic domain walls. *Nat. Mater.* 2019, DOI: 10.1038/s41563-019-0516-z.

(14) Seidel, J. Nanoelectronics based on topological structures. *Nat. Mater.* 2019, 18, 188.

(15) Lytle, F. W. X-Ray diffractometry of low-temperature phase transformations in strontium titanate. *J. Appl. Phys.* 1964, 35, 2212−2215.

(16) Segal, Y.; Garrity, K.; Vaz, C.; Hoffman, J.; Walker, F.; Ismail-Beigi, S.; Ahn, C. Dynamic evanescent phonon coupling across the La$_{1-x}$Sr$_x$MnO$_3$/SrTiO$_3$ interface. *Phys. Rev. Lett.* 2011, 107, 105501.

(17) Nie, Y.; King, P.; Kim, C.; Uchida, M.; Wei, H.; Faeth, B.; Ruf, J.; Ruff, J.; Xie, L.; Pan, X.; et al. Interplay of Spin−Orbit Interactions, Dimensionality, and Octahedral Rotations in Semimetallic SrIrO$_3$. *Phys. Rev. Lett.* 2015, 114, 016401.

(18) Groenendijk, D.; Autieri, C.; Girovsky, J.; Martinez-Velarte, M.; Manca, N.; Mattoni, G.; Monteiro, A.; Gauquelin, N.; Verbeeck, J.; Otte, A.; Caviglia, A.; et al. Spin-orbit semimetal SrIrO$_3$ in the two-dimensional limit. *Phys. Rev. Lett.* 2017, 119, 256403.

(19) Schütz, P.; Di Sante, D.; Dudy, L.; Gabel, J.; Stübinger, M.; Kamp, M.; Huang, Y.; Capone, M.; Husanu, M.-A.; Strocov, V.; et al. Dimensionality-Driven Metal-Insulator Transition in Spin-Orbit-Coupled SrIrO3. *Phys. Rev. Lett.* 2017, 119, 256404.

(20) Carter, J.-M.; Shankar, V. V.; Zeb, M. A.; Kee, H.-Y. Semimetal and topological insulator in perovskite iridates. *Phys. Rev. B: Condens. Matter Mater. Phys.* 2012, 85, 115105.

(21) Chen, Y.; Lu, Y.-M.; Kee, H.-Y. Topological crystalline metal in orthorhombic perovskite iridates. *Nat. Commun.* 2015, 6, 6593.

(22) Kim, H.-S.; Chen, Y.; Kee, H.-Y. Surface states of perovskite iridates AIrO3: signatures of a topological crystalline metal with nontrivial Z 2 index. *Phys. Rev. B: Condens. Matter Mater. Phys.* 2015, 91, 235103.

(23) Fujioka, J.; Yamada, R.; Kawamura, M.; Sakai, S.; Hirayama, M.; Arita, R.; Okawa, T.; Hashizume, D.; Hoshino, M.; Tokura, Y. Strong-correlation induced high-mobility electrons in Dirac semimetal of perovskite oxide. *Nat. Commun.* 2019, 10, 362.

(24) Yamada, R.; Fujioka, J.; Kawamura, M.; Sakai, S.; Hirayama, M.; Arita, R.; Okawa, T.; Hashizume, D.; Hoshino, M.; Tokura, Y. Large Variation of Dirac Semimetal State in Perovskite CaIrO3 with Pressure-Tuning of Electron Correlation. *Phys. Rev. Lett.* 2019, 123, 216601.

(25) Momma, K.; Izumi, F. VESTA 3 for three-dimensional visualization of crystal, volumetric and morphology data. *J. Appl. Crystallogr.* 2011, 44, 1272−1276.

(26) Zhao, J.; Yang, L.; Yu, Y.; Li, F.; Yu, R.; Fang, Z.; Chen, L.; Jin, C. High-pressure synthesis of orthorhombic SrIrO$_3$ perovskite and its positive magnetoresistance. *J. Appl. Phys.* 2008, 103, 103706.

(27) Kronbo, C. H.; Nielsen, M. B.; Kevy, S. M.; Parisiades, P.; Bremholm, M. High pressure structure studies of 6H-SrIrO3 and the octahedral tilting in 3C-SrIrO3 towards A post-perovskite. *J. Solid State Chem.* 2016, 238, 74−82.

(28) Bianchi, U.; Kleemann, W.; Bednorz, J. Raman scattering of ferroelectric Sr$_{1-x}$Ca$_x$TiO$_3$, x = 0.007. *J. Phys.: Condens. Matter* 1994, 6, 1229.

(29) Guzhva, M.; Markovin, P.; Kleemann, W. Spontaneous photorefractive effect in Sr$_{1-x}$Ca$_x$TiO$_3$ (x = 0.014). *Phys. Solid State* 1997, 39, 625−627.

(30) Menoret, C.; Kiat, J.; Dkhil, B.; Dunlop, M.; Dammak, H.; Hernandez, O. Structural evolution and polar order in Sr$_{1-x}$Ba$_x$TiO$_3$. *Phys. Rev. B: Condens. Matter Mater. Phys.* 2002, 65, 224104.

(31) Glazer, A. Simple ways of determining perovskite structures. *Acta Crystallogr., Sect. A: Cryst. Phys., Diffr., Theor. Gen. Crystallogr.* 1975, 31, 756−762.

(32) Brahlek, M.; Choquette, A.; Smith, C.; Engel-Herbert, R.; May, S. Structural refinement of Pbnm-type perovskite films from analysis of half-order diffraction peaks. *J. Appl. Phys.* 2017, 121, 045303.

(33) Evarestov, R. A.; Blokhin, E.; Gryaznov, D.; Kotomin, E. A.; Maier, J. Phonon calculations in cubic and tetragonal phases of SrTiO$_3$: A comparative LCAO and plane-wave study. *Phys. Rev. B: Condens. Matter Mater. Phys.* 2011, 83, 134108.

(34) Liu, J.; Kriegner, D.; Horak, L.; Puggioni, D.; Rayan Serrao, C.; Chen, R.; Yi, D.; Frontera, C.; Holy, V.; Vishwanath, A.; et al. Strain-induced nonsymmorphic symmetry breaking and removal of Dirac semimetallic nodal line in an orthoperovskite iridate. *Phys. Rev. B: Condens. Matter Mater. Phys.* 2016, 93, 085118.

(35) Choquette, A. K.; Smith, C. R.; Sichel-Tissot, R. J.; Moon, E. J.; Scafetta, M. D.; Di Gennaro, E.; Miletto Granozio, F.; Karapetrova, E.; May, S. J. Octahedral rotation patterns in strained EuFeO$_3$ and other Pbnm perovskite films: Implications for hybrid improper ferroelectricity. *Phys. Rev. B: Condens. Matter Mater. Phys.* 2016, 94, 024105.

(36) Horák, L.; Kriegner, D.; Liu, J.; Frontera, C.; Marti, X.; Holý, V. Structure of epitaxial SrIrO$_3$ perovskite studied by interference between X-ray waves diffracted by the substrate and the thin film. *J. Appl. Crystallogr.* 2017, 50, 385.

(37) Zhou, J.-S.; Goodenough, J. B. Intrinsic structural distortion in orthorhombic perovskite oxides. *Phys. Rev. B: Condens. Matter Mater. Phys.* 2008, 77, 132104.

(38) Gruenewald, J. H.; Nichols, J.; Terzic, J.; Cao, G.; Brill, J. W.; Seo, S. S. A. Compressive strain-induced metal−insulator transition in orthorhombic SrIrO$_3$ thin films. *J. Mater. Res.* 2014, 29, 2491−2496.

(39) Matsuno, J.; Ihara, K.; Yamamura, S.; Wadati, H.; Ishii, K.; Shankar, V. V.; Kee, H.-Y.; Takagi, H. Engineering a Spin-Orbital Magnetic Insulator by Tailoring Superlattices. *Phys. Rev. Lett.* 2015, 114, 247209.

(40) Frenkel, Y.; Haham, N.; Shperber, Y.; Bell, C.; Xie, Y.; Chen, Z.; Hikita, Y.; Hwang, H. Y.; Kalisky, B. Anisotropic Transport at the LaAlO3/SrTiO3 Interface Explained by Microscopic Imaging of Channel-Flow over SrTiO3 Domains. *ACS Appl. Mater. Interfaces* 2016, 8, 12514−12519.

(41) May, S.; Kim, J.-W.; Rondinelli, J.; Karapetrova, E.; Spaldin, N.; Bhattacharya, A.; Ryan, P. Quantifying octahedral rotations in strained perovskite oxide films. *Phys. Rev. B: Condens. Matter Mater. Phys.* 2010, 82, 014110.

(42) Guo, W.; Ji, D.; Gu, Z.; Zhou, J.; Nie, Y.; Pan, X. Engineering of octahedral rotations and electronic structure in ultrathin SrIrO3 films. *Phys. Rev. B: Condens. Matter Mater. Phys.* 2020, 101, 085101.

(43) Liu, Y.; Yang, L.; Li, J. Strain-engineered orthorhombic-rhombohedral phase boundary in epitaxial bismuth ferrite films. *J. Appl. Phys.* 2013, 113, 183524.

(44) Bhattacharjee, S.; Bousquet, E.; Ghosez, P. Engineering multiferroism in CaMnO3. *Phys. Rev. Lett.* 2009, 102, 117602.

(45) Bousquet, E.; Cano, A. Non-collinear magnetism in multiferroic perovskites. *J. Phys.: Condens. Matter* 2016, 28, 123001.

(46) Gibert, M.; Viret, M.; Torres-Pardo, A.; Piamonteze, C.; Zubko, P.; Jaouen, N.; Tonnerre, J.-M.; Mougin, A.; Fowlie, J.; Catalano, S.; et al. Interfacial control of magnetic properties at LaMnO3/LaNiO3 interfaces. *Nano Lett.* 2015, 15, 7355−7361.

(47) Caviglia, A. D.; Scherwitzl, R.; Popovich, P.; Hu, W.; Bromberger, H.; Singla, R.; Mitrano, M.; Hoffmann, M. C.; Kaiser, S.; Zubko, P.; et al. Ultrafast strain engineering in complex oxide heterostructures. *Phys. Rev. Lett.* 2012, 108, 136801.

(48) Fowlie, J.; Lichtensteiger, C.; Gibert, M.; Meley, H.; Willmott, P.; Triscone, J.-M. Thickness-Dependent Perovskite Octahedral Distortions at Heterointerfaces. *Nano Lett.* 2019, 19, 4188.

(49) Li, D.; Lee, K.; Wang, B. Y.; Osada, M.; Crossley, S.; Lee, H. R.; Cui, Y.; Hikita, Y.; Hwang, H. Y. Superconductivity in an infinite-layer nickelate. *Nature* 2019, 572, 624−627.

(50) Groenendijk, D.; Manca, N.; Mattoni, G.; Kootstra, L.; Gariglio, S.; Huang, Y.; van Heumen, E.; Caviglia, A. Epitaxial growth and thermodynamic stability of SrIrO$_3$/SrTiO$_3$ heterostructures. *Appl. Phys. Lett.* 2016, 109, 041906.